Received: 16 September 2020 | Revised: 31 October 2020 | Accepted: 31 October 2020

DOI: 10.1002/pls2.10022

RESEARCH ARTICLE

SPE POLYMERS WILEY

Effect of chain extender on structural and mechanical properties of poly(butylene succinate-co-adipate)/halloysite nanotube bionanocomposites

Kalappa Prashantha[1] | **Baralu J. Rashmi**[2]

[1]ACU-Centre for Research and Innovation, Faculty of Natural Sciences, Adichunchanagiri University, B.G. Nagara, India

[2]Department of Chemistry, Faculty of Mathematical and Physical Sciences, M.S. Ramaiah University of Applied Sciences, Bangalore, India

Correspondence
Kalappa Prashantha, ACU-Centre for Research and Innovation, Faculty of Natural Sciences, Adichunchanagiri University, B.G. Nagara, Mandya District 571448, Karnataka, India.
Email: kprashatha@acu.ac.in

Abstract

Bionanocomposites comprising poly(butylene succinate-co-adipate) (PBSA) and halloysite nanotubes (HNTs) were fabricated via melt extrusion using different HNT loadings. These nanocomposites were characterized through Fourier transfer infrared spectroscopy, X-ray diffraction, scanning electron microscopy, and mechanical, thermal, and rheological tests. Adding a chain extender (CE) ensured homogeneous dispersion of HNTs in the PBSA matrix because the epoxy-based CE and HNTs reacted with the carboxyl groups of PBSA, leading to effective interfacial interactions between the matrix and reinforcing filler. Differential scanning calorimetry results revealed that HNTs had a nucleating effect on PBSA, thereby increasing the crystallization of PBSA and percentage crystallinity of the composites. Nevertheless, the CE did not cause any change in the crystallinity of the nanocomposites. Further, the thermal stability of PBSA without and with the CE reduced, depending on the HNT loading. The HNTs and CE also increased the melt strength of PBSA. Additionally, HNTs and CE enhanced the mechanical properties owing to the increased molecular weight and formation of long-chain branched structures.

KEYWORDS

chain, extender, halloysite nanotubes, morphology, nanocomposites, poly(butylene succinate-co-adipate)

1 | INTRODUCTION

Poly(butylene succinate-co-adipate) (PBSA) is an eco-friendly polyester that has attracted considerable interest owing to its biodegradability, high flexibility, melt processability, and thermal and chemical resistance, thus proving effective for diverse applications.[1–3] PBSA is a random copolymer of poly(butylene succinate) (PBS) and adipate with properties comparable to those of polyolefins.[4] However, some drawbacks limit its use, such as, poor mechanical strength, gas-barrier properties, and thermal stability. Therefore, incorporating nanofillers into polymer matrices is another way to produce new nanocomposites with desired properties.[5] Zhiguo Qi et al.[6] studied the dynamic rheological properties of attapulgite (ATP)-reinforced PBSA nanocomposites. They found that adding nanoclays increased the viscoelastic properties of PBSA. S.S. Ray et al.[7] prepared PBSA/organically modified montmorillonite (OMMT) nanocomposites and reported that the essential properties of the PBSA improved because

of OMMT reinforcement. S.S. Ray et al.[8] also studied the influence of organically modified synthetic fluorine mica (OSFM) on the properties OSFM/cold-crystallized PBSA nanocomposites with results indicating that the uniform distribution of OSFM in the PBSA matrix enhances the cold crystallization temperature of the nanocomposites. However, achieving a homogeneous dispersion of organosilicates such as montmorillonite in polymer matrices is extremely difficult.[9]

Halloysite nanotubes (HNTs) are natural nanotubes with aluminosilicate ($Al_2Si_2O_5$) $(OH)_4.nH_2O$ crystallites. They have attracted considerable interest from the research community because of their high aspect ratio, excellent biocompatibility, low cost, abundance, high mechanical strength, low hydroxyl group density on the surface, and chemical similarity to kaolin.[10–18] Melt extrusion was used to prepare different types of HNT-based polymer nanocomposites. Ismail et al.[19] studied the morphological and mechanical properties of HNT-filled ethylene-propylene-diene monomer nanocomposites. They found that the tensile strength and ductility of these nanocomposites were enhanced simultaneously by the addition of HNTs, particularly at high HNT loadings. K. Prashantha et al.[10,20] deduced that HNTs can function as eco-friendly and sustainable reinforcements for thermoplastics. Rybinski et al.[21] and Du et al.[22] reported that HNTs could reduce flammability and enhance thermal stability of HNT-filled nanocomposites.

Generally, PBSA has low melt strength and mechanical properties. These limitations are directly related with the linear structure of PBSA. Using a chain extender (CE) during processing condensation polymers such as polyesters and polyamides[23–25] has proved effective and economical. Thus, a CE can counterbalance the low molecular weight of PBSA. Furthermore, a styrene-acrylic multifunctional-epoxide oligomeric CE commercially known as Joncryl® has been utilized for processing polyesters. Various grades of these compounds are commercially available with different glass transition temperatures, molecular weights, and epoxide concentrations. The epoxy groups in these compounds act as the primary reactive groups, which can merge with the end groups of polyesters to enhance their viscosity and molecular weight.[26]

However, there are no studies that have comprehensively analyzed the influence of HNTs and CE on the properties of PBSA-based nanocomposites. Therefore, in this work, Joncryl® ADR-4368 was used as the CE to improve the properties of PBSA/HNT nanocomposites while maintaining their properties end use properties. PBSA/HNT and CE-added PBSA/HNT (CE-PBSA/HNT) nanocomposites were fabricated through masterbatch dilution using a twin-screw extruder. The properties of the fabricated nanocomposites were determined to evaluate their suitability for potential applications as biomaterials.

2 | EXPERIMENTAL

2.1 | Materials

PBSA (PBE 001) was purchased from Nature Plast, France. HNTs having a length of approximately 1.2 μm, density of 205 g/cm^3, and an average diameter of 80 nm were purchased from Natural Nao Inc. Joncryl® ADR 4368C, a solid oligomeric CE, was obtained from BASF, Florham Park, NJ 07932. Before processing, all the materials were dried under vacuum at 80°C for 8 hr to remove moisture. All the materials were used as received.

2.2 | Fabrication of PBSA/HNT nanocomposites

Masterbatch dilution was used to prepare PBSA/HNT nanocomposites. The masterbatch was prepared by mixing 10 wt% of HNTs with PBSA granules in a twin-screw extruder (HAAKE Poly lab OS, Thermo scientific). The length/diameter (L/D) ratio of the screws was 40, their diameter was 16 mm, and the screw speed was 60 rpm. The temperature profile of the extruder varied from 120 to 130°C from the hopper to the die. The extrudate filaments were fed through a pelletizer (SGC 25-E4, Scheer, Germany) to convert them into tiny pellets. The prepared pellets were dried overnight in a vacuum oven at 80°C to eliminate moisture for further applications. Then, the masterbatch was diluted with neat PBSA to yield nanocomposites filled with 2, 4, 6, and 8 wt% of HNTs.

Further, to study the influence of the CE on these PBSA/HNT nanocomposites 1 wt% of the CE was incorporated through melt processing using the twin-screw extruder, as described above.

Dried nanocomposite pellets were injection-molded (HAAKE MiniJet II, Thermo scientific) to obtain standard test specimens for measuring the rheological and tensile properties. The melt temperature ranged from 105 to 110°C. The mold temperature was 60°C, and the holding pressure was 450 bar. All the specimens were kept at 25°C with 50% relative humidity for a week before further usage.

2.3 | Attenuated total reflection- Fourier transform infrared spectra (ATR-FTIR)

The FTIR spectra of PBSA/HNT nanocomposites without and with the CE were recorded on a Thermo Scientific Nicolet 380 spectrometer. The measuring resolution was 4 cm^{-1} in the range of 50–4000 cm^{-1}.

2.4 | Morphology- scanning electron microscopy (SEM)

SEM (S-4300SE/N, Hitachi, Japan) was utilized to examine the microstructure and dispersion of the nanotubes in the PBSA/HNT nanocomposites with an accelerating voltage of 5 kV. Prior to SEM analysis, the prepared samples were cryo-fractured by dipping them in liquid nitrogen and subsequently coated with a thin gold layer.

2.5 | X-Ray diffraction (XRD)

XRD measurements were recorded on a Bruker AXS D8 advanced diffractometer with cobalt radiation ($\lambda = 1.789$ Å) operating at 40 mA and 35 kV. The samples were scanned at diffraction angles (2θ) ranging from 10 to 40° a scanning speed of 0.2°/min.

2.6 | Thermogravimetric analysis (TGA)

Thermal stability of the nanocomposites was studied using TGA (Mettler Toledo analyzer, France). The samples (approximately 5–10 mg) were heated from 30 to 600°C at a heating rate of 20°C/min under nitrogen atmosphere.

2.7 | Differential scanning calorimetry (DSC)

DSC measurements of the nanocomposites were conducted with using a calorimeter (TA Instruments, Mettler Toledo, France) under nitrogen flow. Each sample weighing 5–10 mg was sealed in an alumina pan and heated from −60 to 150°C (first heating scan) with a heating rate of 10°C/min and then cooled from 150 to −60°C at a cooling rate of 10°C/min to eliminate thermal history. The samples were subsequently heated up to 150 °C at 10°C/min (second heating scan). Thermal properties such as the crystallization temperature (T_c), melting temperature (T_m), crystallization enthalpy (ΔH_c), and melting enthalpy (ΔH_m) were determined from the thermograms. The degree of crystallinity (X_c) was calculated using Equation (1):

$$\chi_c = \frac{\Delta H_m}{\Delta H\circ_m (1 - w_t)} \quad (1)$$

where ΔH_m is the melting enthalpy, ΔH°_m is the melting enthalpy of 100% crystalline PBS equal to 110.3 J/g[1] and w_t is the filler weight fraction in the nanocomposites.

2.8 | Melt rheology

A HAAKE Mars rheometer III fitted with a plate-plate having a diameter of 35 mm was used to conduct melt rheological measurements on the injection-molded samples. All measurements were obtained under nitrogen atmosphere at 120°C to prevent degradation of the polymer. The linear viscoelastic behavior of each sample was determined using an angular frequency of 1 rad/s.

2.9 | Tensile properties

The tensile tests were performed as per ISO 527 standards on the injection-molded nanocomposite specimens. Tensile properties such as the Young's modulus, tensile strength, and % elongation at break were measured using an Intron universal testing machine (Model 1185, Instron) with a crosshead speed of 10 mm/min^{-1} maintaining a gage length of 50 mm at 25°C and 50% RH. All the reported values are the averages of the values obtained using five specimens for each composition.

3 | RESULTS AND DISCUSSION

3.1 | ATR-FTIR

Figures 1A,B show the FTIR spectra recorded for the neat PBSA, HNTs, PBSA/HNT nanocomposites with different HNT contents, and CE-PBSA/HNT nanocomposites. As observed in Figure 1A, HNTs show characteristic peaks at 3703 and 3629 cm^{-1}, corresponding to stretching vibrations of the —OH group; further, the peaks at 1034 and 1012 cm^{-1} corresponding to the stretching vibrations of the Si-O group, and the peak at 910 cm^{-1} represents the bending vibrations of the Al—OH group. PBSA shows a characteristic peak at 1670 cm^{-1}, indicating stretching of the C═O group. The peak at 1416 cm^{-1} is attributed to stretching of the —COO- group, and that at 1103 cm^{-1} represents stretching of the C—O—C group. The IR peaks of HNTs at 1034 and 1012 cm^{-1} (Figure. 1A) corresponding to the hydroxyl groups of HNTs are not present in the spectra of the PBSA/HNT nanocomposites. The disappearance of these characteristic peaks clearly indicates effective interfacial interactions between the HNTs and PBSA matrix owing to the formation of hydrogen bonds between the hydroxyl groups of the HNTs and carbonyl groups of the PBSA matrix.

The characteristic IR peaks at 848 and 914 cm^{-1} correspond to the cyclic epoxide group in the pure CE (Figure 1B). These two peaks disappear in the spectra of the CE-PBSA/HNT nanocomposites. This was attributed

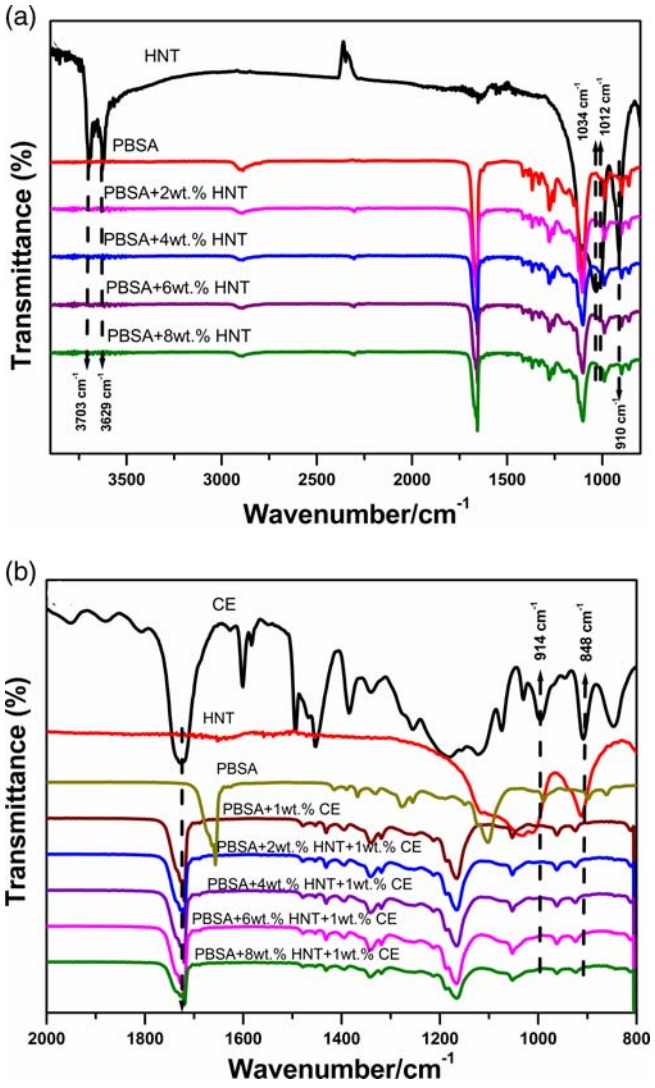

FIGURE 1 FTIR spectra of PBSA and various PBSA/HNT nanocomposites A, without CE and B, with CE

to the opening of the epoxide rings during their reactions with the carboxyl and/or hydroxyl end groups of PBSA.

V. Ojijo[27] has reported that the epoxide groups in the CE react with carboxylic/hydroxyl end groups present in PBSA, potentially forming a long-chain branched structure. The reaction includes opening of the epoxide ring, which requires the abstraction of carboxyl groups and hydrogen to form secondary hydroxyl groups and establish ester bonds between the polymer and CE. The newly developed hydroxyl side groups and the initial hydroxyl end groups compete with the epoxides for undergoing esterification. Chain branching and possibly crosslinking could occur owing to the existence of the hydroxyl side groups.

Accordingly, in the CE-PBSA/HNT nanocomposites (Figure 1B), as the HNT content increased, the corresponding peaks of the nanocomposites shifted from 1670, 1416, and 1103 cm^{-1} to higher wavelengths of 1724, 1431, and 1165 cm^{-1}, respectively, compared with the peaks obtained for samples without the CE. This shift was due to the uniform distribution of HNTs in the PBSA matrix, and addition of the CE could have further promoted the interactions between the HNTs and PBSA matrix.

3.2 | Morphology

Figures 2A,B show the SEM micrographs depicting the fracture surfaces of neat PBSA, and the PBSA/HNT and CE-PBSA/HNT nanocomposites as a function of the HNT loading. The nanocomposites with and without the CE show satisfactory dispersion of the HNTs owing to hydrogen bonding, as observed in the FTIR results. The interfacial interaction between the HNTs and PBSA matrix is effective. However, adding the CE further improved these interfacial interactions (Figure 2B), leading to better HNT dispersion in the PBSA matrix than that observed in the PBSA/HNT nanocomposites without the CE. Therefore, adding a CE could influence the filler dispersion and matrix morphology of nanocomposites. Moreover, the CE and HNTs reacted with the carboxyl groups of PBSA, leading to excellent interfacial interactions between the matrix and reinforcing filler.

The XRD curves of the PBSA/HNT nanocomposites without and with the CE as a function of the HNT loading are shown in Figures 3A,B. The characteristic diffraction peaks of HNTs are observed at 13.91°, 23.16°, and 28.58°, and those of PBSA are observed at 26.27°, 30.44°, and 33.30°. The intensity of the XRD peaks of the PBSA/HNT nanocomposites notably decreased and shoulder peaks were observed, indicating structural changes due to the interaction of hydroxyl groups of HNT through H-bonds with PBSA. As a function of the HNT loading, the peak amplitudes remained almost unaltered, but the position of the peaks shifted toward lower diffraction angles, suggesting an apparent change in the crystalline structure of the PBSA.

Within increasing HNT loadings along with the addition of the CE (Figure 3B), the intensities and positions of the peaks remained the same in all nanocomposites compared to those of the neat HNT peaks. This means the HNTs had almost no effect on the crystalline structure of PBSA in the presence of the CE.

3.3 | Thermal analysis

Tables 1A,B describe the crystallization and melting behavior, and Figures 5A,B shows second heating and

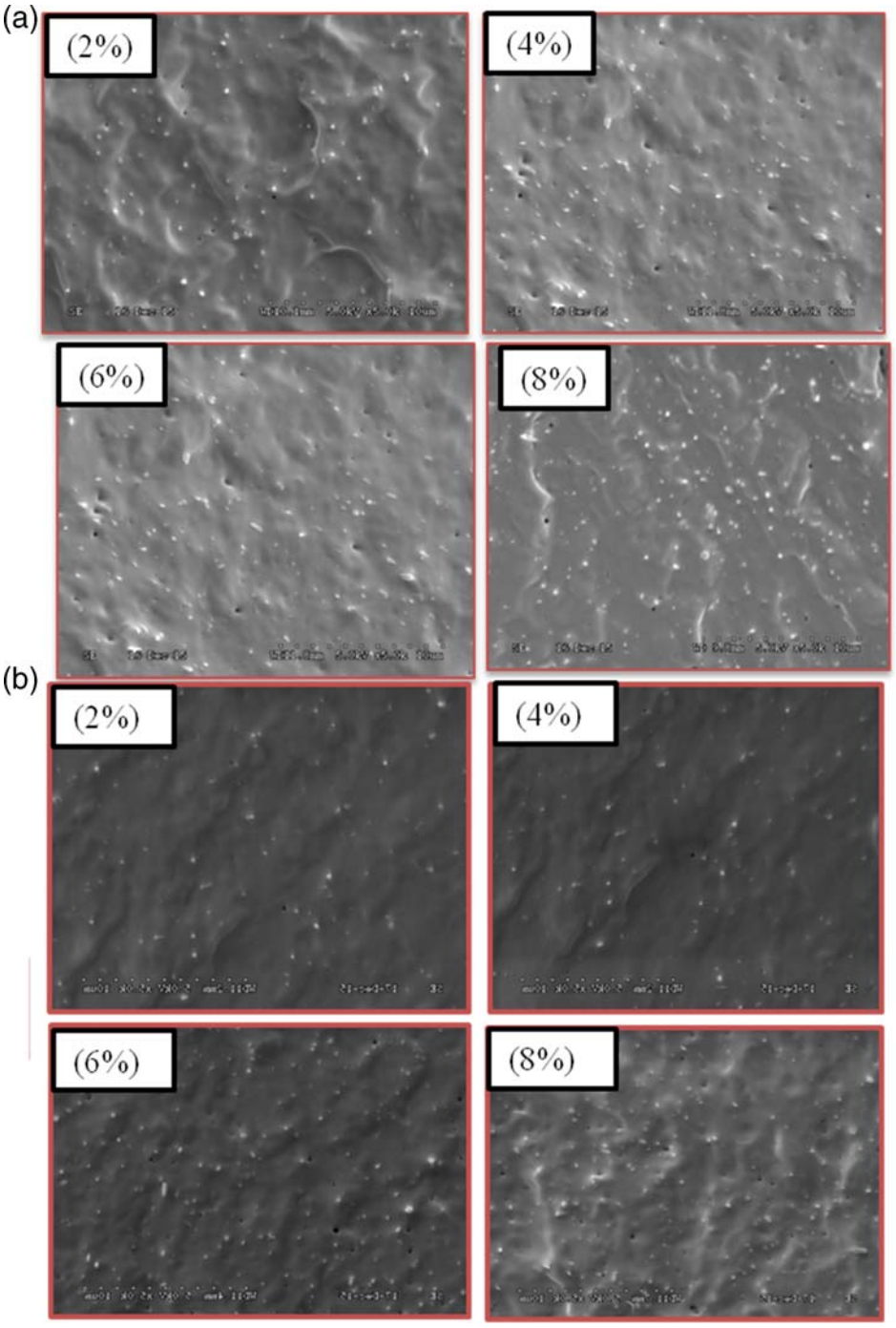

FIGURE 2 SEM micrographs showing fractured surfaces of PBSA and PBSA/HNT nanocomposites with various HNT contents, with and without CE. A, PBSA and PBSA/HNT nanocomposites without CE and B, PBSA/HNT nanocomposites with CE

first cooling DSC thermograms of neat PBSA, and PBSA/HNT and CE-PBSA/HNT nanocomposites. The glass transition temperature (T_g) of PBSA marginally increased on incorporating HNTs, indicating reasonable interactions between the PBSA matrix and HNT surfaces. Further, melting peaks were not affected noticeably upon adding HNTs. The measured melting points were extremely close to each other. In Figures 4A,B, two endothermic melting peaks are observed, denoted as $T_{m1}$and T_{m2}, for neat PBSA and PBSA/HNT nanocomposites. According to the melt-recrystallization model,[3] melting and recrystallization occur concurrently during heating, indicating the transformation of incomplete/small lamellae into more organized lamellae with adequate thermal stability in the melt state. The crystallization temperature (T_c) of pure PBSA was 37.88°C. As the HNT loading increased, the T_c of PBSA gradually shifted to higher values. Therefore, HNTs functioned as nucleating agents, increasing the crystallization rate of pure PBSA through a heterogeneous nucleation process. Meanwhile, the crystallization enthalpies (ΔH_c) of PBSA/HNT nanocomposites also increased compared to that of pure PBSA. Moreover,

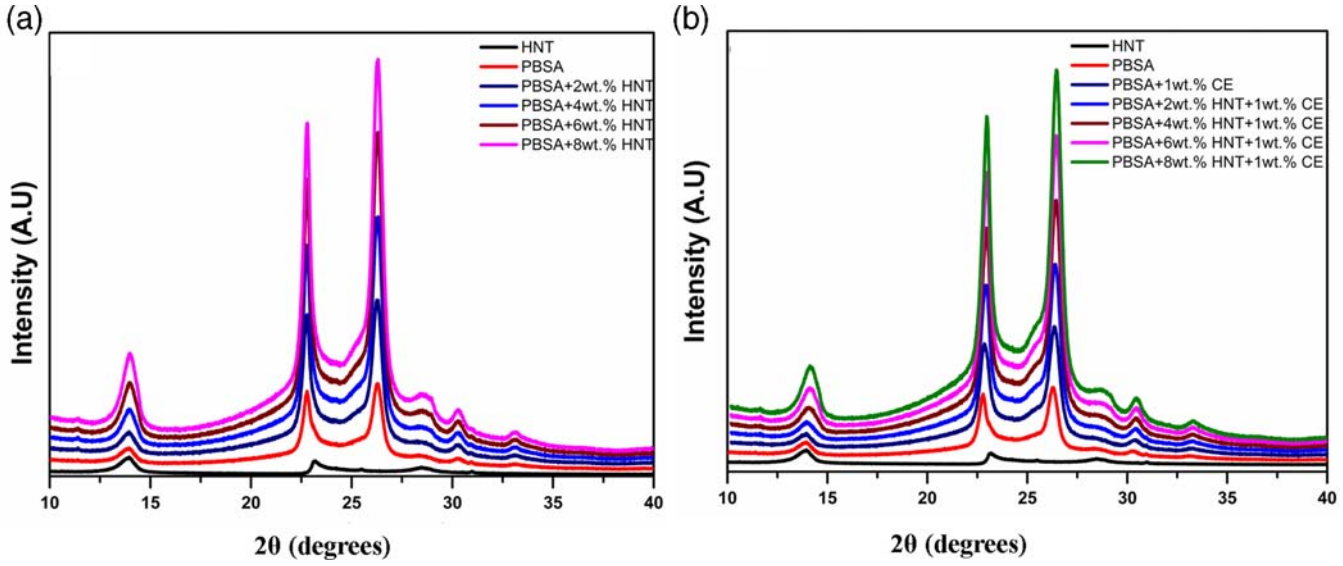

FIGURE 3 XRD patterns of HNT, neat PBSA, and PBSA/HNT nanocomposites A, without CE and B, with CE

TABLE 1 DSC thermograms of neat PBSA and PBSA/HNT nanocomposites (a) second heating and first cooling and (b) with CE second heating and first cooling with 1 wt% CE

(a)						
Sample	T_g (°C)	T_C (°C)	T_{m1} (°C)	T_{m2} (°C)	ΔH_m (J/g)	X_c (%)
PBSA	−43.30	37.88	—	88.17	45.45	41.37
PBSA + 2 wt% HNT	−42.51	50.0	79.30	89.21	50.16	46.40
PBSA + 4 wt% HNT	−42.49	51.21	79.31	89.16	52.20	49.29
PBSA + 6 wt% HNT	−41.35	51.38	79.31	88.73	53.24	51.34
PBSA + 8 wt% HNT	−41.31	52.07	79.97	88.56	54.54	53.74
(b)						
Sample	T_c (°C)	ΔH_c (J/g)	T_{m1} (°C)	T_{m2} (°C)	ΔH_m (J/g)	X_c (%)
PBSA	49.87	42.07	77.90	87.13	44.60	40.23
PBSA + 2 wt% HNT	50.07	42.48	79.79	88.54	46.82	42.87
PBSA + 4 wt% HNT	48.57	40.51	77.51	88.98	43.32	39.67
PBSA + 6 wt% HNT	48.50	39.97	76.78	88.88	41.72	38.20
PBSA + 8 wt% HNT	47.11	39.51	75.96	88.26	39.11	35.81

T_{m2}, which corresponds to the reorganization of the crystallites with high thermal stability, moved toward lower values as a function of the HNT loading. This is because the rate of recrystallization was higher than the rate of melting, indicating the HNTs improved the recrystallization of PBSA.

When the CE was added to PBSA (Figures 4C,D, and Table 1B), a slight increase in the T_c of PBSA was observed, indicating an increase in the molecular weight. However, when HNTs were incorporated, the T_c decreased in the composites without the CE. Formation of nonlinear molecules during the reaction between PBSA and the CE inhibited the crystallization process, thereby decreasing the T_c. Nevertheless, the variations observed in the T_c, X_c, and T_m are significant, suggesting that 1 wt% of the CE has limited influence on the crystallization processes of PBSA, thus agreeing with the findings of Jennifer et al..[28]

Figure 6A shows the TGA thermograms of PBSA and PBSA/HNT nanocomposites with different HNT loadings, indicating the thermal decomposition temperatures recorded at 5% weight loss ($T_{5wt\%}$). It is evident that after formation of the nanocomposites, the thermal stability of PBSA decreased with the increasing HNT loading, and the

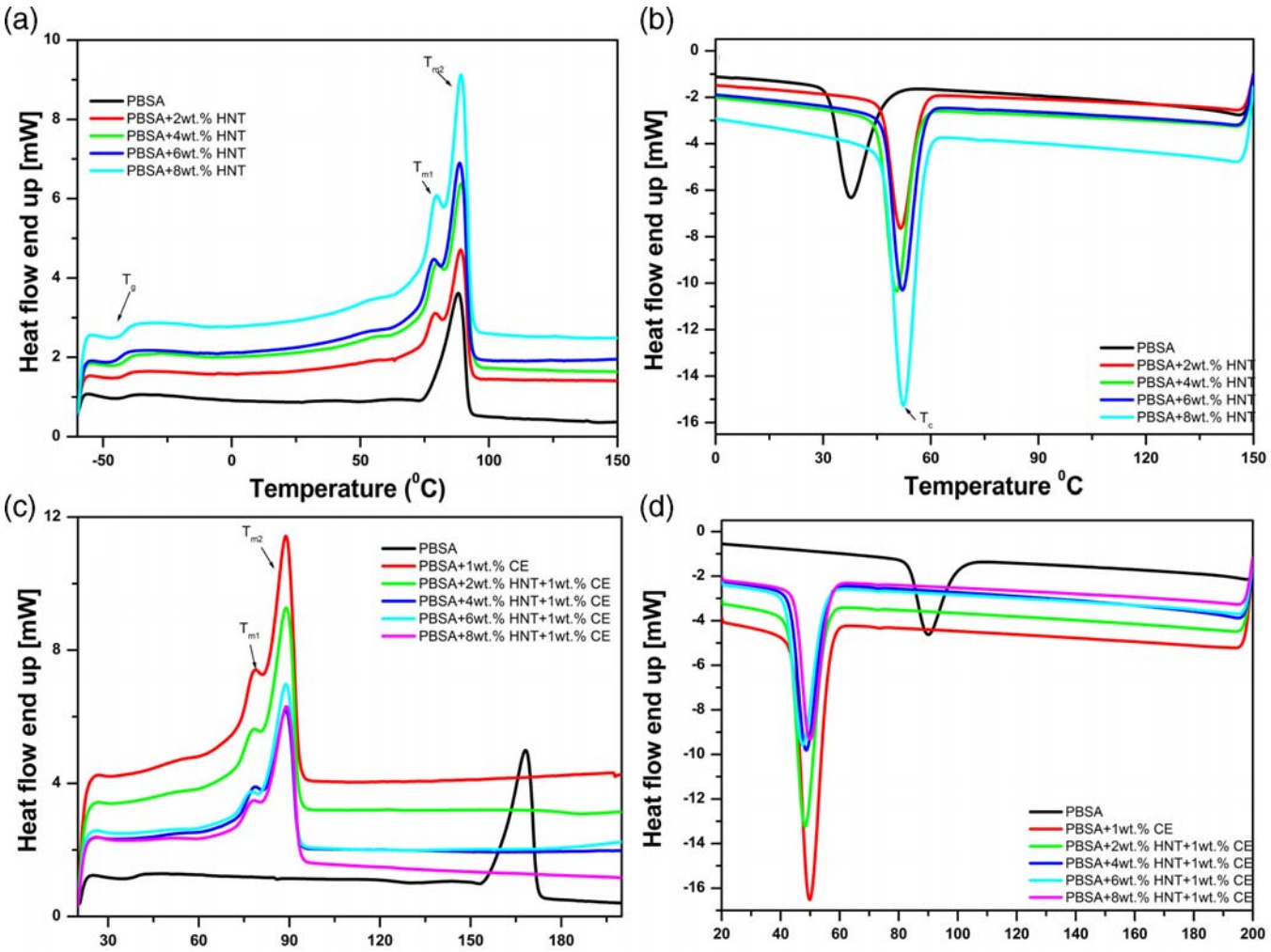

FIGURE 4 DSC thermograms of PBSA/HNT nanocomposites with different HNT contents. A, Second heating of PBSA/HNT without CE, B, Cooling of PBSA/HNT without CE, C, Second heating of PBSA/HNT with CE, and D, Cooling of PBSA /HNT with CE

degradation onset temperature significantly decreased as the HNT loading increased. This indicates that the HNT has no effective barrier effect due to the dehydration of HNTs.[29] Figure.5A indicates only one main decomposition step for the PBSA/HNT nanocomposites with a HNT loading at 5% weight loss. Moreover, the weight loss at the maximum degradation temperatures decreased as the HNT loading increased. The degradation temperatures of the nanocomposites were 447.07, 443.39, 439.92, 435.21, and 433.58°C at HNT loadings of 2, 4, 6, and 8 wt%, respectively, compared with 448.30°C obtained for neat PBSA. Defeng Wu et al.[30] for PLA/clay nanocomposites and L.N. Carli also reported similar results for PHBV/HNT nanocomposites.[31]

Addition of the CE to the PBSA with the HNTs (Figure 5B) did not cause significant changes in the thermal degradation properties when compared to that observed without the CE owing to the lack of synergy between the CE and HNTs. The CE was partially adsorbed on the clay surface, thereby reducing its effect on the thermal stability of the nanocomposites.[32] Moreover, the hydroxyl groups present in the HNTs could hydrolyze the ester groups in PBSA during melting at elevated temperatures. This might have decreased the degradation rate of the PBSA/HNT composites, thus hindering the thermal stabilizing effect of the HNTs. Accordingly, the decomposition temperatures of PBSA/HNT nanocomposites decreased gradually with increasing HNT contents. A similar phenomenon was also observed by Jennifer G-A et al.[28] when examining the effect of CE on PHBV/HNT nanocomposites.

3.4 | Melt rheology

Rheological characterization was carried out to understand the effect of the HNTs and CE on viscoelastic behavior of the PBSA nanocomposites. Frequency sweeps were

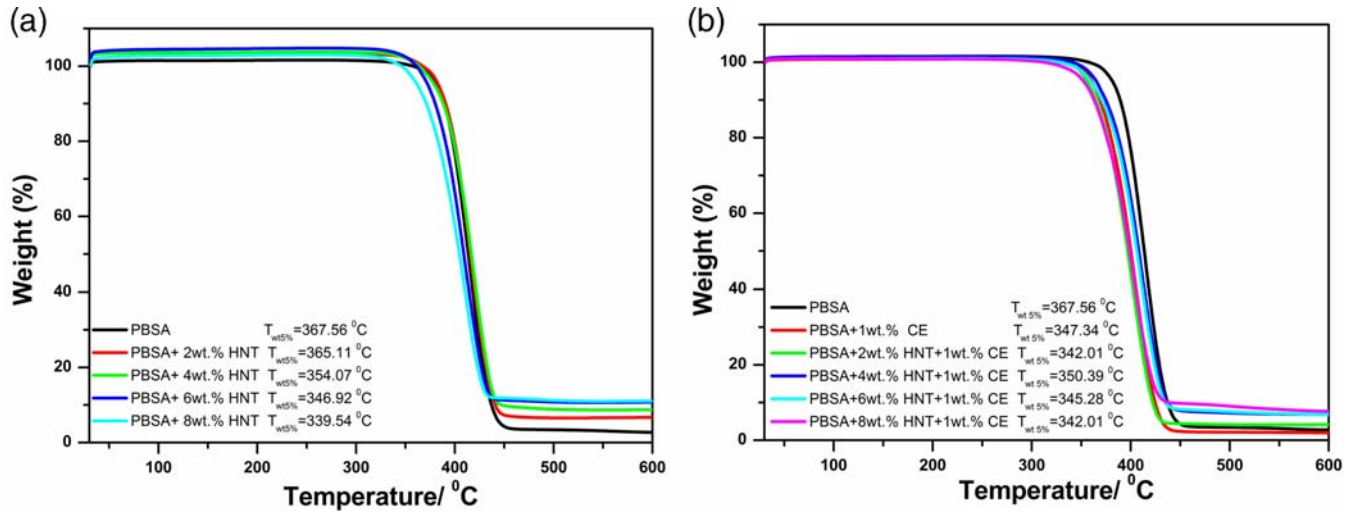

FIGURE 5 TGA thermograms of PBSA and PBSA/HNT nanocomposites: A, without CE and B, with CE

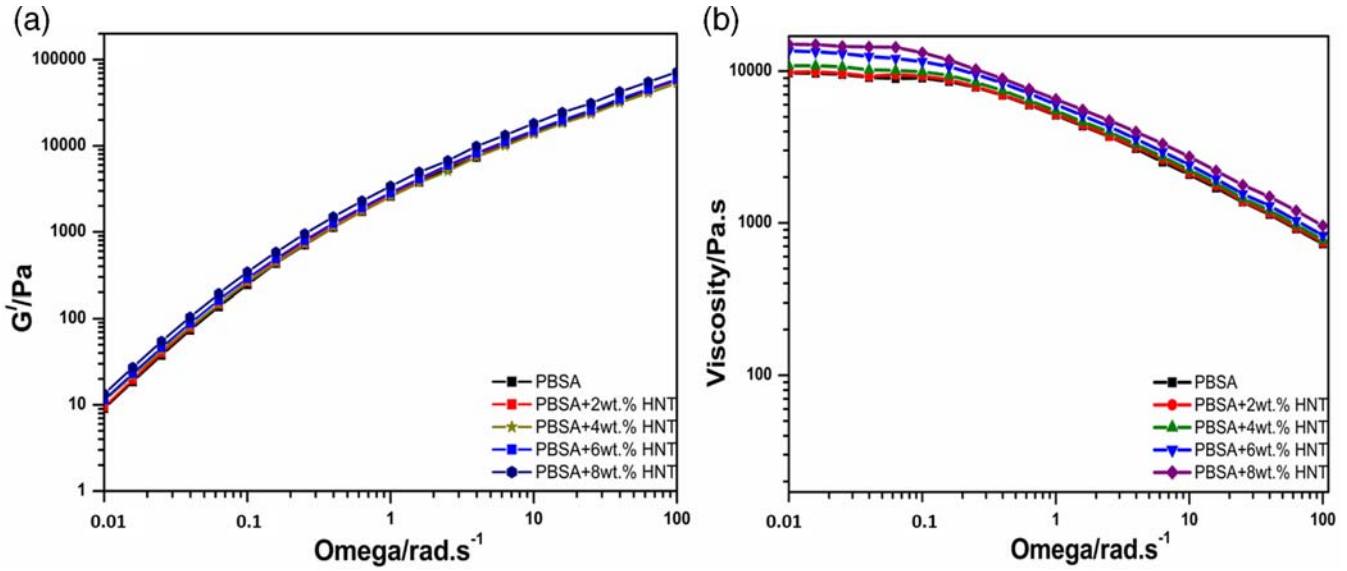

FIGURE 6 Frequency dependence of A, storage moduli $G^{l}(\omega)$ and B, complex viscosities of PBSA and various PBSA/HNT without CE

performed at 120°C from 0.1 to 1 rad/s. The loss moduli, $G^{l}(\omega)$, and complex viscosities of neat PBSA, PBSA/HNT nanocomposites, CE-PBSA, and CE-PBSA/HNT nanocomposites are presented in Figures 6 and 7. Figure 6A clearly shows that in the high-frequency zone, all the nanocomposites exhibit similar viscoelastic behaviors except for a slight increase in $G^{l}(\omega)$ with increases in the HNT loading. Thus, the chain relaxation observed is virtually unaffected by the addition of HNTs. However, in the low-frequency region, $G^{l}(\omega)$ exhibits weak frequency dependence with increases in the HNT loading. Figure 7B shows the changes in the complex viscosities (η^*) of the PBSA and PBSA/HNT nanocomposites at low and high viscosity PBSA in Figure 7B. In the low-frequency region, PBSA displays a frequency-independent horizontal viscosity zone corresponding to Newtonian flow followed by a decrease in π^* as the frequency increased, indicating pseudo-plastic behavior. This behavior was observed even in the nanocomposite with 8 wt% HNTs. We attributed this to the moderate PBSA backbone interactions with the HNT surfaces that led to a substantial confinement of the matrix chains on the HNT surfaces owing to excellent dispersion of the HNTs in the PBSA matrix, as observed in the FTIR and SEM results (Figures 1 and (Figure 2). Owing to their highly anisotropic nature, the dispersed HNTs exhibited intramolecular interactions that finally resulted in the formation of microscopic domains or structures. The change in the viscosity of the polymer nanocomposites was

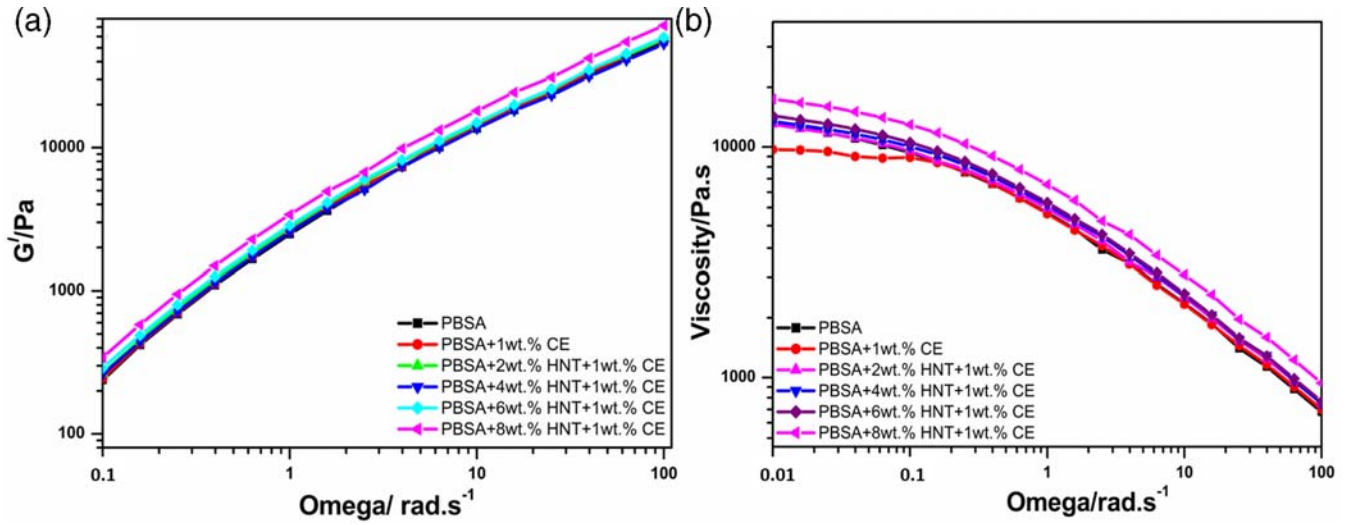

FIGURE 7 Frequency dependence of A, storage moduli $G^{I}(\omega)$ and B, complex viscosities of PBSA and various PBSA/HNTs with CE

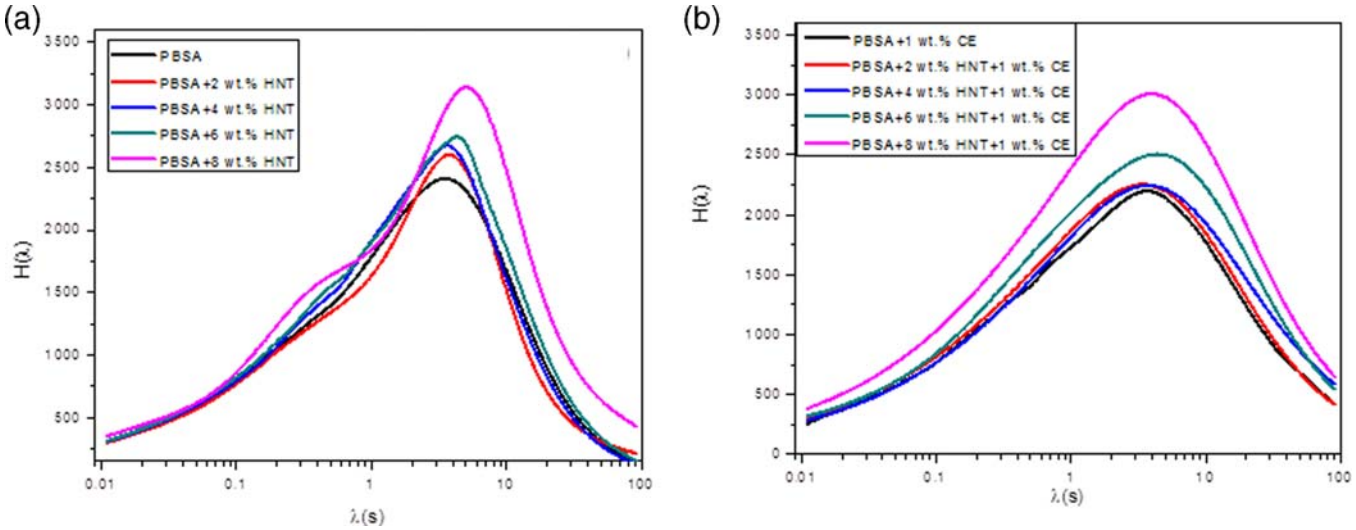

FIGURE 8 Relaxation spectrum of PBSA and PBSA/HNT nanocomposites: A, without CE and B, with CE

attributed to the flow hindrance of the polymer chains in the molten state owing to the presence of the nanotubes.

Furthermore, the CE-PBSA/HNT nanocomposites (Figure 7) showed higher complex viscosity and storage modulus values in the low-frequency region compared to those observed for the nanocomposites without the CE. This could be attributed to the HNT dispersion in the presence of the CE, as confirmed through morphology observations. In fact, well-dispersed nanotubes have a large interfacial area, thus enabling stronger interactions between the polymer matrix and HNTs in the nanocomposites. Such interactions in nanocomposites hinder the movement of macromolecular chains, and this is reflected by an increase in their viscosity and elasticity.

In addition, post-treatment of rheological data using Honerkamp and Weese Equations[33] was performed to better understand the effect of the CE on the nanocomposite properties. Using Equations (2 and 3), the weighted relaxation spectrum, λ H (λ), was calculated from the linear relaxation spectrum, H(λ). This spectrum shows the chain relaxation time distributions of the samples with and without the CE.

$$G' = \int_0^\infty \frac{H(\omega\lambda))^2}{1+(\omega\lambda))^2} d(ln\lambda) \quad (2)$$

$$G'' = \int_0^\infty \frac{H(\omega\lambda)}{1+(\omega\lambda))^2} d(ln\lambda) \quad (3)$$

where "ω" is the angular frequency and "λ" is the relaxation time.

TABLE 2 Tensile properties of neat PBSA and PBSA/HNT nanocomposites without and with CE

Sample	Without CE			With CE (1%)		
	Tensile modulus (MPa)	Tensile strength (MPa)	Elongation at break (%)	Tensile modulus (MPa)	Tensile strength (MPa)	Elongation at break (%)
PBSA	285.65 ± 20.47	26.93 ± 2.09	345.36 ± 12.79	294.58 ± 6.31	29.29 ± 0.14	329.59 ± 10.51
PBSA + 2 wt% HNT	319.53 ± 19.88	28.51 ± 2.9	391.30 ± 13.10	334.71 ± 17.59	31.04 ± 0.82	370.36 ± 14.11
PBSA + 4 wt% HNT	334.48 ± 23.85	29.14 ± 1.97	410.01 ± 16.17	342.39 ± 28.28	32.45 ± 1.47	375.63 ± 15.13
PBSA + 6 wt% HNT	345.80 ± 11.50	30.33 ± 1.36	445.62 ± 16.11	368.48 ± 12.52	34.07 ± 2.13	405.16 ± 16.03
PBSA + 8 wt% HNT	351.51 ± 32.08	30.51 ± 1.96	462.50 ± 12.56	384.84 ± 25.01	34.59 ± 1.06	445.47 ± 13.05

In the PBSA and PBSA/HNT nanocomposites, two relaxation peaks were observed, corresponding to the linear and branched macromolecular chains of PBSA. In the neat PBSA, relaxation of the linear and branched chains occurred at 0.36 and 3.6 s, respectively. One interesting observation was that the relaxation time for linear chains decreased with the addition of HNTs (Figure 8A). On the other hand, incorporating HNTs increased the relaxation time for branched chains. Moreover, increases in the HNT loading broadened the relaxation peak (Figure 8A). These findings indicate that HNTs significantly influence PBSA relaxation. Such relaxation mechanisms are associated with conformational changes in polymer backbones, which are active below and above the glass transition temperature.[34] In particular, the local dynamics processes occurring because of the strong hydrogen bonding networks between the HNTs and PBSA affect the relaxation characteristics of the HNT/PBSA nanocomposite systems.

Further, in the CE-PBSA and CE-PBSA/HNT nanocomposites, we observed only one relaxation peak corresponding to the relaxation of the branched chains (Figure 8B). Hence, melt extrusion is effective in branching the PBSA chains. The relaxation peak for the CE-PBSA appeared at 3.8 s, and the addition of HNTs slightly increased the relaxation time of CE-PBSA. Adding HNTs together with the CE further strengthened the hydrogen bonding in the nanocomposite system, resulting in higher chain stability and increased elasticity, and consequently a slow stress relaxation process. We also noticed that the relaxation peak broadened following the incorporation of the HNTs.

3.5 | Tensile properties

Table 2 presents tensile properties of PBSA, and PBSA/HNT and CE-PBSA/HNT nanocomposites. Adding HNTs enhances the tensile properties of PBSA. The tensile modulus of PBSA containing 2 wt% HNTs is 334.53 MPa, which is higher than 285.65 MPa observed for neat PBSA. The modulus gradually increased with the HNT loading and a significant increase to 384.84 MPa was observed at 8 wt% HNT loading. This can be attributed to better adhesion between the PBSA matrix and HNTs. Better adhesion improves the load bearing properties of the nanocomposites; HNTs function as load carriers and enable increased stress transfer at the interface.

The tensile strength of PBSA also increased after nanocomposite formation (Table 2). The tensile strength increased to 31.04 MPa from 29.31 MPa (neat PBSA) for the nanocomposite with 2 wt% HNTs. As the HNT loading increased, the tensile strength increased, and a substantial increase to 34 MPa was observed at 6 wt% HNT loading. Nevertheless, the improvement in tensile strength with further addition of HNTs is not very significant. With HNT reinforcement, the percentage elongation at break for PBSA marginally decreased. The elongation at break for PBSA decreased from 347.5% to 345.30% after nanocomposite formation with 2 wt% of HNTs. Moreover, the elongation at break did not decrease significantly (less than 10%) even with 8 wt% of HNTs. Thus, we could obtain unique PBSA/HNT nanocomposites with high tensile strength without sacrificing ductility.

In addition, general increments in the tensile modulus and strength were observed for the CE-PBSA/HNT nanocomposites, albeit lower than those of the PBSA/HNT nanocomposites. However, CE-PBSA/HNT nanocomposites exhibited a higher elongation at break than PBSA/HNT nanocomposites. This is because a CE increases the molecular weight and enables the development of long-chain branched structures.[35] This long-chain branching increases the intensity of entanglements in polymer structures,[36,37] thus impeding the slippage and alignment of the chains after elongation. Yim et al.[38] reported similar results for ultra-high molecular weight polyethylene. Nevertheless, in the PBSA/HNT nanocomposites containing the CE, improved HNT dispersion facilitates interfacial associations between the HNTs and PBSA in addition to the enhanced molecular weight of PBSA. Thus, stress transfer from the

PBSA matrix to the HNTs increases, resulting in improved tensile strength and modulus of these nanocomposites. Based on the above results, we can infer that incorporating a CE enhances the mechanical properties of nanocomposites.

4 | CONCLUSIONS

PBSA/HNT nanocomposites were successfully fabricated through masterbatch melt blending. Incorporating the multifunctional-epoxy-based CE enhanced the molecular weight of PBSA and modified its linear chain structures to long-chain branched structures. These modifications increased the melt strength, mechanical properties, and crystallinity of PBSA. The FTIR, SEM, and XRD measurements indicated that favorable nanocomposite morphologies were achieved by incorporating the HNTs and CE (owing to excellent dispersion of HNTs within the PBSA matrix). The CE improved the tensile modulus of PBSA and percentage elongation at break of the PBSA/HNT nanocomposites. The thermal stability of PBSA reduced on adding the HNTs and CE because the decomposition temperature and activation energy for thermal degradation steadily decreased as the HNT loading increased. DSC analyses revealed that the overall crystallization temperature and crystallinity of PBSA increased on adding HNTs, indicating that HNTs had a nucleating effect on the PBSA matrix. However, the overall crystallization temperature and crystallinity were not altered by adding the CE. According to the XRD data, the HNTs and CE slightly modified the crystal structure of PBSA. Nevertheless, the HNTs strongly influenced the rheological properties of the nanocomposites, especially in the low-frequency region. The dispersion of the HNTs in the presence of the CE resulted in highest complex viscosity and storage modulus. Thus, adding a CE can improve filler dispersion in nanocomposites, provided it is added judiciously. Finally, the fabricated nanocomposites can have applications as biodegradable materials.

DATA AVAILABILITY STATEMENT

The data that support the findings of this study are available from the corresponding author upon reasonable request.

ORCID

Kalappa Prashantha https://orcid.org/0000-0001-8350-3970

Baralu J. Rashmi https://orcid.org/0000-0001-7742-6657

REFERENCES

[1] S. Charlon, S. Marais, E. Dargent, J. Soulestin, J. Sclavons, M. N. Follain, *Phys. Chem. Chem. Phys.* **2015**, *17*, 29918.

[2] W. Abdallah, A. Mirzadeh, V. Tan, M. R. Kamal, *Nanomaterials* **2019**, *9*, 29.

[3] S. S. Ray, J. Bandyopadhyay, B. Mosto, *Polym. Degrad. Stabil.* **2007**, *92*, 802.

[4] D. R. Ishioka, E. Kitakuni, Y. Ichikawa, Y. Doi, A. Steinbuchel, Eds., Wiley-VCH, Weinheim. *4*, 275, **2002**,.

[5] M. Nofar, R. Salehiyan, U. Ciftci, A. Jalali, A. Durmuş, *Compos. Sci. Tech.* **2020**, *107661*, 182.

[6] Z. Qi, J. Chen, B. Guo, Z. Liu, Proceedings of 2012 International Conference on Mechanical Engineering and Material Science (MEMS 2012)

[7] S. S. Ray, B. Mosto, K. Okamot, *Macromol. Mater. Eng.* **2005**, *290*, 759.

[8] S. S. Ray, B. Mosto, *Macromol. Chem. Phys.* **2006**, *207*, 1207.

[9] M. A. Paul, C. Delcourt, M. Alexandre, P. Degee, F. Monteverde, A. Rulmont, P. Dubois, *Macromol. Chem. Phys.* **2005**, *206*, 484.

[10] K. Prashantha, M. F. Lacrampe, P. Krawczak, *eXPRESS Polym. Lett.* **2011**, *5*, 295.

[11] H. Schmitt, N. Creton, K. Prashantha, J. Soulestin, M. F. Lacrampe, P. Krawczak, *Polym. Eng. Sci.* **2015**, *55*, 573.

[12] M. Liu, B. Guo, M. Du, D. Jia, *Appl. Phys. A* **2007**, *88*, 391.

[13] K. Prashantha, M. F. Lacrampe, P. Krawczak, J. Appl, *Polym. Sci.* **2013**, *130*, 313.

[14] D. M. Steeves, R. Farrell, R. Jo, *Ann, J.Bioba.Mater.Bioen* **2007**, *1*, 94.

[15] M. X. Liu, Y. Zhang, C. C. Wu, S. Xiong, R. Zhou, *Int. J. Bio. Macromo.* **2012**, *51*, 566.

[16] J. M. Duan, R. C. Liu, T. Chen, B. Zhang, J. D. Liu, *Desalination* **2012**, *293*, 46.

[17] U. A. Handge, K. Hedicke-Hochstotter, V. Altstadt, *Polymer* **2010**, *51*, 2690.

[18] N. Oburoglu, N. Ercan, A. Durmus, A. Kasgoz, *J. Macromol. Sci.* **2012**, *51*, 860.

[19] H. Ismail, P. Pasbakhsh, M. N. Fauzi, A. AbuBakar, *Polym. Test.* **2008**, *27*, 841.

[20] H. Schmitt, P. K. Rashantha, J. Soulestin, M. F. Lacrampe, P. Krawczak, *Carbo. Polym* **2012**, *89*, 920.

[21] P. R. G. Janowska, T. Chimica, *Thermochimica Acta* **2012**, *549*, 6.

[22] M. Du, B. Guo, D. Jia, *Euro. Polym. J.* **2006**, *42*, 1362.

[23] W. G. Blasius, G. A. Deeter, *Polymer* **2006**, *B2*, 10.

[24] J. A. Cicero, J. R. Dorgan, S.F. Dec, D.M. Knauss, D. M. *Polym. Degrad. Stab. 78*, 95. **2002**.

[25] W. Fan, Y. Zhao, A. Zhang, Y. Liu, Y. Cao, J. Chen, J. *J. Appl. Polym. Sci.* **2015**, *132*, 41561.

[26] S. R. Sahas, E. B. Rathi, S. L. Hsu, S. L. Golub, G. H. Ling, M. J. Tzivanis, *Polymer* **2014**, *6*, 1232.

[27] V. Ojijo, S. S. Ray, *Polymer* **2015**, *80*, 1.

[28] G.A. Jennifer, S.S. Estefania, G.P. Jos, C. Luis, *J. Appl. Polym. Sci.* **2016**, *133*, 42390.

[29] T. S. Gaaz, A. B. Sulong, A. A. H. Kadhum, A. A. Al-Amiery, M. H. Nassir, A. H. Jaaz, *Molecules* **2017**, *22*, 838.

[30] D. Wu, L. Wu, L. Wu, M. Zhang, *Polym. Degrad. Stab.* **2006**, *91*, 3149.

[31] L. N. Carli, J. S. Crespo, R. S. Mauler, *Compo.Part A: Appl. Sci. Manuf.* **2011**, *42*, 1601.

[32] S. Murugesan, T. Scheibel, *Adv. Funct. Mater.* **2020**, *30*, 1908101.

[33] J. Honerkamp, J. Weese, *Rheol. Acta* **1993**, *32*, 65.

[34] S. Fotiadou, C. Karageorgaki, C. Chrissopoulou, K. Karatasos, I. Tanis, D. Tragoudaras, B. Frick, S. H. Anastasiadis, *Macromolecules* **2013**, *46*, 2842.

[35] C. N. Najafi, M. C. Heuzey, P. J. Carreau, P. M. Wood-Adams, *Polym. Degrad.Stabil.* **2012**, *97*, 554.
[36] M. A. Kennedy, A. J. Peacock, L. Mandelkern, *Macromolecules* **1994**, *27*, 5297.
[37] G. G. Lin, H. H. Shih, P. C. Chai, S. Hsu, *Polym. Eng. Sci.* **2002**, *42*, 2213.
[38] C. I. Yim, K. J. Lee, J. Y. Jho, K. Choi, *Polym. Bull.* **1999**, *42*, 433.

How to cite this article: Prashantha K, Rashmi BJ. Effect of chain extender on structural and mechanical properties of poly(butylene succinate-co-adipate)/halloysite nanotube bionanocomposites. *SPE Polymers*. 2020;1:101–112. https://doi.org/10.1002/pls2.10022